Journal of Oceanography, Vol. 64, pp. 115 to 130, 2008

The Upper Ocean Response to a Moving Typhoon

YALING TSAI, CHING-SHENG CHERN* and JOE WANG

Institute of Oceanography, National Taiwan University, P.O. Box 23-13, Taipei 106, Taiwan, R.O.C.

(Received 4 January 2007; in revised form 10 September 2007; accepted 18 September 2007)

The upper ocean response to the translation speed of typhoons is studied using a three-dimensional primitive equation model. Similar models studied previously have applied stability criteria rather than the diffusion term to simulate the vertical mixing process. This study retains the diffusion term and uses the level-2 turbulence closure scheme to estimate the vertical eddy viscosity. The model results indicate that in the forced period, the mixed-layer temperature decrease is greater for a slow-moving storm due to stronger upwelling caused by the longer residence time. A fast-moving storm can attain a similar cooling intensity in the wake period if its residence time allows the wind to resonate with the current. The significant downward momentum diffusion and advection in the first few inertial periods of these events leads to strong, persistent inertial pumping throughout the upper ocean in the wake period. The mixed layer is further cooled by turbulent mixing supported by vertical current shears. Meanwhile, the upper thermocline exhibits a compensating temperature increase. The vertical transfer magnitude and penetration scale are smaller in the slow-moving case, when the inertial motion decays rapidly. The model results also indicate that the dominant cooling process can be inferred from the non-dimensional storm speed. However, this value may be misleading for rapidly moving storms in which the current response is so distant from the storm that little wind work is performed on the ocean.

Keywords:
· Typhoon,
· mixed layer cooling,
· inertial motion,
· entrainment mixing,
· resonant response.

1. Introduction

The upper ocean's response to a moving typhoon has attracted considerable attention. A distinctive feature of this response is the decrease in the sea surface temperature (SST) to the right of a moving storm. The SST decrease can affect storm forecasting (Cione and Uhlhorn, 2003) and it is also important in climate research for estimating the ocean's heat transport (Emanuel, 2001). Tropical cyclones are strong, localized weather systems. Their characteristics affect the strength of ocean cooling and inertial oscillations arising from their passage. Since a storm travels across the ocean with the wind rotating around the storm center, it may produce a wind forcing that varies at a frequency close to the inertial frequency, given a correctly matched size and translation speed. The inertial motion and cooling in the upper ocean are enhanced during such wind-current resonant events (Crawford and Large, 1996).

The conventional approach to simulating such wind-generated inertial motions adopts the slab mixed layer (ML) model, as in the classic study of Pollard and Millard (1970), who proposed a two-layer slab ML model in which the subsurface drag against the imposed wind stress is modeled as a linear damping term. The damping coefficient, which has a dimension of $(\text{time})^{-1}$, is linearly proportional to the entrainment velocity at the base of the ML. Instead of using one linear damping term, the subsequent model study of Chang and Anthes (1978) explicitly specified individual forcings, such as the pressure gradient force or horizontal advection, to better describe the mechanism responsible for the storm-induced ocean cooling. However, they found that entrainment mixing remains the dominant process in reducing the ML temperature, as is shown by the results of the field experiments (Jacob *et al*., 2000; D'Asaro, 2003). The entrainment in the slab ML model can only be estimated through the calculation of the entrainment rate parameterized by various schemes. Generally, an entrainment rate parameterization is meant to model the turbulent stress associated with the momentum transfer between the ML and the layer below. However, this leads to an inherent limitation for the slab ML model, in that larger entrainment cooling will lead to faster decay of the inertial current. The slab ML model is thus unable to depict those

* Corresponding author. E-mail: cschern@ntu.edu.tw

events that consist of both significant cooling and prolonged inertial currents in the ML. An example of such events is reported in Zedler *et al*. (2002), who found a temperature decrease of 3°~3.5°C and *e*-folding decay times of 14.9 days for the inertial currents at 25 m depth due to the passage of Hurricane Felix.

In addition to the above-mentioned limitation, the fact that the 2-layer slab model confines all mixing in the ML is seemingly inconsistent with the observations. The ocean's density profile is generally more sophisticated than a simple two-layer structure. Taking the ocean's vertical structure into consideration, Price (1983) and Wada (2002) both use a model containing one ML and a few other layers. The importance of the thermocline is recognized and discussed in these models. Besides adding layers to the slab ML model, another type of approach models the vertical structure of hurricane-induced ocean response by summing the first few baroclinic modes. Shay *et al*. (1989), for example, found that a model based only on the first four forced modes can explain about 70% of the current variance. However, as discussed in Price (1983), such a normal mode solution requires intensive numerical calculations and is not applicable when the response is not modal or wave-like. Price *et al*. (1994) therefore adopted a three-dimensional (3-D) primitive model to study the upper ocean's response to three hurricanes. The vertical mixing in this model was treated by forcing the model to satisfy three stability criteria: static stability, ML shear flow stability, and stratified shear flow stability. Although the model provides fairly good simulations of the current structure in the ML, some features resulting from the local mixing, e.g. cooling in the ML and warming in the thermocline (Zedler *et al*., 2002), cannot be depicted in this model using bulk stability criteria.

Among the storms analyzed by Price *et al*. (1994), Hurricane Norbert was specifically discussed because substantial thermocline currents were observed in that case. In his study (and also in normal model solutions), the ML and the thermocline are coupled through the horizontal pressure gradient, and Price estimated that approximately 35% of the kinetic energy in Norbert was transferred downward through this coupling. It is noteworthy that Norbert was an intense, relatively small storm in which the pressure gradient effectively connected the thermocline and the ML. On the other hand, the connecting mechanism for large, fast-moving storms was not discussed in Price's study due to a lack of relevant observations. The large, fast storms, as defined in Greatbatch (1984), have translation speeds U_h greater than the first baroclinic mode wave speed c_1 and half-width of its cross-track response length scale larger than the scale defined by c_1/f (f is the inertial frequency). We may infer a small, negligible horizontal pressure gradient term for storms within this limit. The pressure coupling is important in the Norbert case because the ratio U_h/c_1 is only 1.5 and the response length scale and the scale c_1/f are about the same (~42 km). A question then arises regarding the response to those large and fast storms: is there still any significant coupling between the ML and the thermocline, at least in the first few inertial periods (IP) after the arrival of a storm?

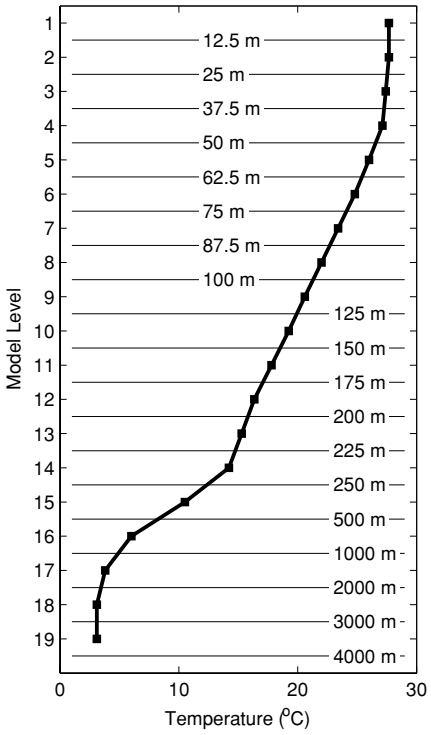

Fig. 1. Model vertical layer arrangement and initial temperature profile.

Considering the issues set out above, in this study we examine the ocean cooling induced by large, fast-moving storms using a 3-D primitive equation model with higher vertical resolution in the ML and the thermocline. Unlike the integral form of the vertical mixing used by Price *et al*. (1994), the model retains the diffusion terms and uses the turbulence closure scheme to estimate the vertical eddy viscosity coefficient. Cases of storms having different translation speeds are considered to study the conditions favorable for the occurrence of wind-current resonance and the dominant cooling mechanisms. The sensitivity of the storm-induced upper-ocean cooling to its vertical mixing efficiency is also discussed.

2. Model Formulation and Numerical Experiments

The model used in this study is modified from Semtner and Mintz (1977) and includes the Boussinesq, hydrostatic, and rigid-lid approximations. The model is

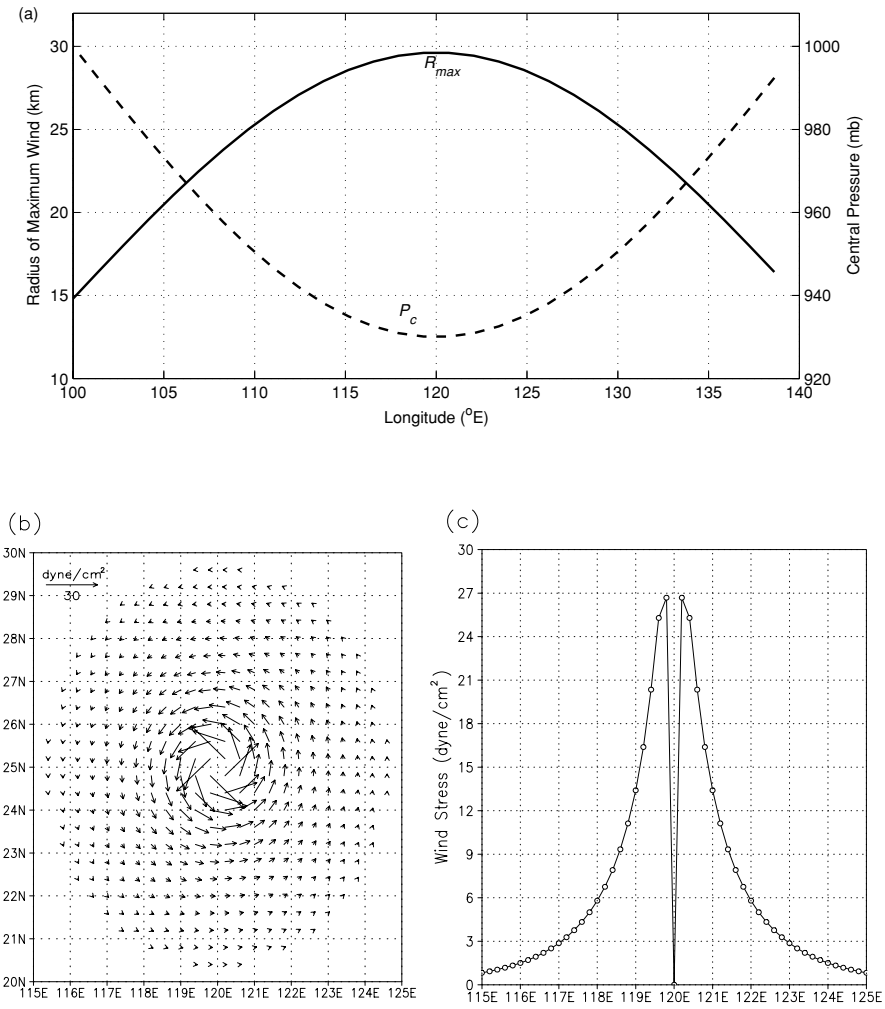

Fig. 2. (a) Radius of maximum wind ($R_{\max}$) and central pressure (P_c) used in storm wind calculation across the model domain. (b) Calculated wind stress distribution when the storm center is located at (120°E, 25°N). (c) As (b) but shown in a cross-section through the storm in the along-track direction.

bounded by 100 and 140°E meridians and 10 and 40°N parallels with a horizontal resolution of 0.2° (approximately 22 km). The vertical layer thickness varies at higher resolutions in the mixed layer and the thermocline (Fig. 1). A simplified model basin and ocean condition are adopted, wherein the modeled ocean is 4-km deep and is initially quiescent with vertical stratification only. The initial vertical stratification is a typical temperature profile observed in the South China Sea (Fig. 1). The salinity is fixed at 35 PSU in the model through out the calculation. As for the surface boundary condition, since the ML cooling is mostly due to the entrainment (D'Asaro, 2003) and reliable surface heat flux data under an active storm are not available, we adopt a simple, constant SST boundary condition. The influence of surface heat flux on the mixing can be found in Wada (2002), while this study focuses on the wind-current resonance effect only.

Two storm cases are considered with identical wind stress distributions but different translation speeds U_h (3.33 m/s and 6.65 m/s). In both cases, the storm moves steadily to the west along 25°N. In case C1 (U_h = 6.65 m/s), the storm sweeps across the domain in 7 days, while in case C2 (U_h = 3.33 m/s) it takes 14 days. It is worth noting that the speed of motion in C1 is much faster than the first baroclinic mode wave speed c_1, which is about 2 m/s in the experiment, while the speed in C2 is relatively closer to c_1. In addition, the internal radius of deformation c_1/f (~32 km) in the experiment is also much smaller than the cross-track response scale, which will be discussed later. In other words, the storm case used in this study satisfies the condition of a large, fast storm as defined by Greatbatch (1984).

The storm wind fields are calculated based on the Rankine Vortex theory (Holland, 1980), in which a sym-

Table 1. List of cases and their storm-related parameters studied in this study. *Av* is the vertical eddy viscosity determined by the turbulence closure scheme in all cases except in cases C1a and C2a, where a constant value is used. T_s is the storm residence time estimated by counting the period when the wind stress is larger than 1 dyne/cm^2. k is the ratio of the local inertial period (28.3 hr at 25°N) to the storm residence time.

Storm case	U_h (m/s)	Av (cm^2/s)	T_s (hr)	k
			(at 119°E, 25°N)	
C1	6.65	Variable	39	0.73
C1a	6.65	5	39	0.73
C2	3.33	Variable	75	0.38
C2a	3.33	5	75	0.38
C3	4.46	Variable	51	0.56
C4	9.31	Variable	24	1.18

metric wind stress distribution is parameterized by the radius of the maximum wind, $R_{\max}$, and the central pressure of the storm, P_c. The magnitude of these storm parameters is a half sine wave through the time/longitude span, as shown in Fig. 2(a), and the storm size/intensity increases and decays over its course to the west. The specified maximum/minimum value of $R_{\max}/P_c$ is not rare: on average 18 tropical cyclones reached this value in the Northwest Pacific from 2004 to 2006. The maximum wind stress calculated based on these values is about 27 dyne/cm^2 (Figs. 2(b) and (c)), which is about the strength of a strong tropical cyclone. The reduction of the storm size and strength near the model's eastern and western boundaries serves to diminish the effect from the boundary to the model results in the domain center. The analyses presented in the next section are mainly based on the model results of the cross-track transect at 119°E when the storm intensity reaches its maximum.

To assess the influence of the storm's translation speed on the ocean's mixing efficiency, each case is studied with both constant (5 cm^2/s) and variable vertical eddy viscosity, estimated using the turbulence closure scheme described in Mellor and Durbin (1975). This scheme follows the level-2 parameterization in which the turbulent energy equation is formulated such that it balances the shear production, the buoyancy production and dissipation. All the numerical experiments are summarized in Table 1. In the following discussion the time axis is converted to units of local IP. The initial point (0 IP) is the time when the wind stress is greater than 1 dyne/cm^2. This value is also used to define the end of the forced period of the ocean response as the storm wind stress magnitude falls below it; the response is then referred to as the relaxation wake period.

3. Results

3.1 Temperature response

The simulation results for both cases indicate that the maximum sea surface cooling (SSC) appears on the right (north) side of the track at approximately 25.5°N. The SSC forms patches along the track in both cases as a result of the convergence/divergence of inertial currents (i.e., inertial pumping) generated by the storm passage (Fig. 3). In both cases, the along-track scale of the cooling patches, as reported in Price (1983), is close to $U_h \times$ IP and is thus larger in case C1. In regard to the cross-track scale of the patches, although the radius of the maximum wind (a widely used scale parameter) is the same in both cases, still C1 appears to have a larger scale than C2. The length of the half-width of the cross-track response scale is about 100 km and 50 km in C1 and C2, respectively, both of which values are larger than the internal radius of deformation. Besides the horizontal SSC scale, the difference in the vertical displacements of the isotherms is also distinct. Comparison of the temperature profiles at 119°E transect for both cases at 5.7 IP (1 IP ~ 28 hours at 25°N) after the storm's arrival indicates that the maximum cooling occurs at 25.5°N, where C2 is colder than C1 at depths above 200 m (Fig. 4). It is observed that in C1, a secondary bulge appears along 27°N, while in C2 the lifting of the isotherms is less significant at the corresponding latitude. This second cooling center in C1, shown in the upper 50-m mean cooling time series plot at 119°E transect, reaches 2°C at approximately 4 IP. Thereafter, a time lag of approximately 0.6 IP between the second and the first cooling center becomes evident (Fig. 5). Another distinct difference between the two cases is the maximum cooling. In C1 the maximum cooling increased in the wake period, whereas in C2 it decreased after 5 IP. In addition, a time lag to the south within the cooling center (greater than –3°C) appears after 3 IP in C2, whereas in C1 the cooling variation is symmetric about the center. In other words, the cooling in C2 is less biased to the right of the storm track, but a phase difference exists across the cold patch. A similar phase lag is also seen in figure 7 of Chang and Anthes (1978), which shows a snapshot of the vertical velocity distribution in their model for the slow-moving storm case. This feature results from the Ekman pumping, which is no longer negligible in the slow-moving case. It is effective near the storm center and the induced upwelling strength is proportional to the duration of the storm. Therefore, the upwelling is clear near the storm center in the slow-moving case, but its response lags behind the inertial pumping in the right sector of the storm.

To further examine the difference between the cases, Fig. 6 shows the upper 400-m temperature response from 0 to 7 IP at the maximum cooling center of transect 119°E.

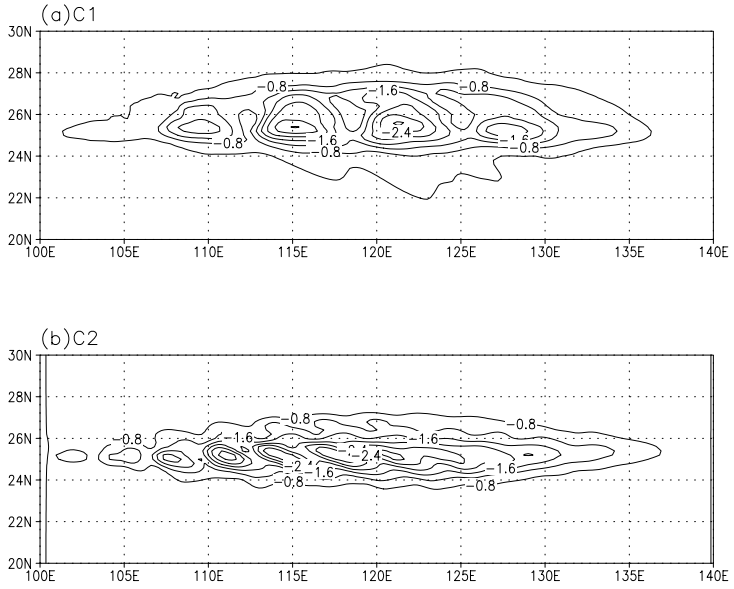

Fig. 3. Temperature anomalies (°C) at model level 2 for C1 (a) and C2 (b) as the storm is about to leave the domain. Contour interval is 0.4°C.

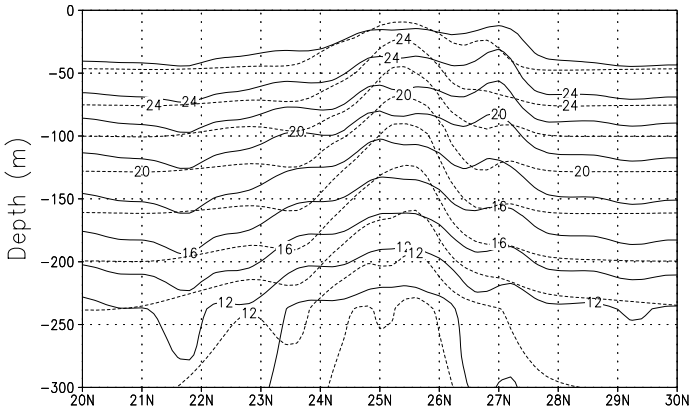

Fig. 4. Upper 300-m temperature field (°C) for C1 (solid line) and C2 (dashed line) at 119°E transect at 5.7 IP after the arrival of the storm.

The temperature field starts to respond to the wind only after about half of the forced period has elapsed. Two cooling maxima are found in the vertical profile: one is in the upper thermocline close to the base of the ML, where the temperature gradient is large; the other is at a depth of approximately 250 m, where the vertical velocity is large. Notably, over the 7-IP time span, the maximum cooling in C2 occurs during the wind-forced period, while in C1 it occurs later in the wake period. The maximum temperature decrease near the ML base in C2 reaches 5°C in the forced period. This cooling, besides the transient response during 2~3 IP, persists until 4 IP and then reduces to 4.5°C between 4~5 IP. In C1, the direct wind force causes a temperature decrease of 4°C, while an additional 1°C cooling occurs later in the wake period and persists after 5 IP. For the cooling center in the lower thermocline, the temperature decrease for cases C1 and C2 reaches approximately 3 and 3.5°C, respectively, in the forced period. In the subsequent wake period the cooling increased in both cases and the maximum decrease achieved was 5°C. The maximum cooling then decreases to 4.5°C after 4 IP in C2 but persists in C1 until 7 IP.

Besides the cooling magnitude, the time evolution of the temperature change clearly indicates that more persistent oscillations are induced in the upper ocean in C1,

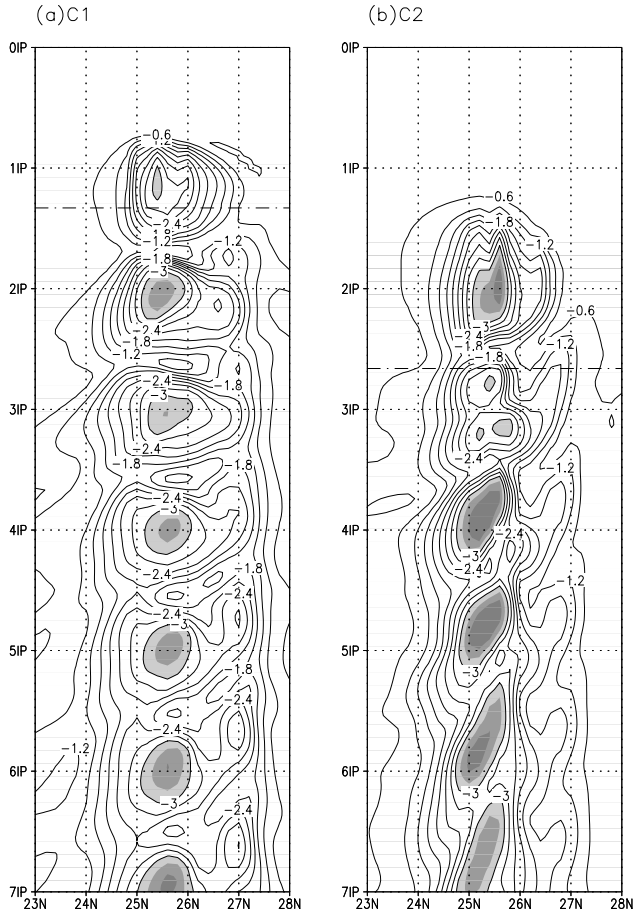

Fig. 5. Upper 50-m mean cooling (°C) for C1 (a) and C2 (b) at 119°E, 23~28°N from 0~7 IP. Contour interval is 0.3°C. Cooling exceeding 3°C is depicted by shaded areas. Dot-dashed lines mark the end of the wind-forced period and the beginning of the relaxation wake period.

while the fluctuations decay after 4 IP in C2. This difference can be better studied through the vertical structure of the horizontal velocity (Fig. 7). It appears that the velocity profile in C1 assumes the first baroclinic mode structure at about 6 IP. The node resides at depths of around 60~100 m, corresponding to the upper cooling center where the temperature gradient is large. When the ML and thermocline are coupled in this first mode structure, the inertial motion persists longer and remains strong. In C2, much less energy is transferred into the thermocline and no such mode structure is observed. The current velocity decays rapidly both vertically and with time.

Our result is consistent with the conclusions of Geisler (1970), who stated that the degree of wake response depends on the storm residence time, which is large for fast-moving/short-stay storms. Geisler's study also stated that an appreciable wake is generated only if the passage time of the region of strong wind stress curl is less than half a pendulum day (one IP). In our study, since the wind-forced period experienced at (119°E, 25°N) is closer to the IP in C1 (Table 1), the rates of wind energy input to the currents are higher than in C2, according to the study of Crawford and Large (1996). The mixing and cooling processes associated with the storm events of variant translation speeds were examined by Chang and Anthes (1978) using a slab ML model, and by Wada (2002) using a ML ocean model with more layers in the vertical. In their models, the entrainment rate is parameterized by the imposed wind stress, buoyancy effect, and vertical current shears. Both studies show that the magnitude of ML cooling was smaller for faster-moving storms; however, the integration time is short in both studies. When the integration time is not long, the upwelling in the forced period is an important mechanism for ML cooling, particularly for the slow-moving storm. Its strength directly reflects the magnitude of the typhoon's wind stress and residence time. Our study further reveals that the cooling may be enhanced in the wake period for a faster-moving storm if wind-current resonance occurs. The main cooling mechanism in such a case is then the turbulent mixing associated with the storm-induced, near-inertial motions in the upper ocean. Figure 8(a) shows the vertical profile of the estimated vertical eddy diffusivity from 0~6 IP. It is clear that the diffusivity extends deeper in the vertical and is larger in the wake period in the C1 case. Such significant mixing in the wake period was reported in the study of Jacob *et al*. (2000), who investigated the ocean's response to Hurricane Gilbert, finding that the shear-induced mixing contributed most to the ML dynamics and persisted up to the third day after the storm's passage. To summarize, in our simulations the slow-moving storm cools the ocean faster, but the fast-moving storm achieves the same effect within a few IPs, as demonstrated by the 6~7 IP mean temperature profiles for C1 and C2 in Fig. 8(b).

It is worth commenting on the feasibility of the clamped SST condition used in our model study. In order to properly simulate the upper ocean's thermal structure, one needs to know either the surface heat flux or the SST. However, both these items of information are not easy to estimate under an active typhoon. We then face the situation that the near surface temperature field cannot be determined exactly. Some previous observations have indicated that the upper ocean cooling under a typhoon is primarily due to the upwelling and entrainment of cold water beneath the surface mixed layer. Hence, as a first step, we may adopt a zero heat flux condition at the surface. However, this condition will result in an artificially long lifetime for the cooling event, which is the main issue that we want to investigate in this paper. Furthermore,

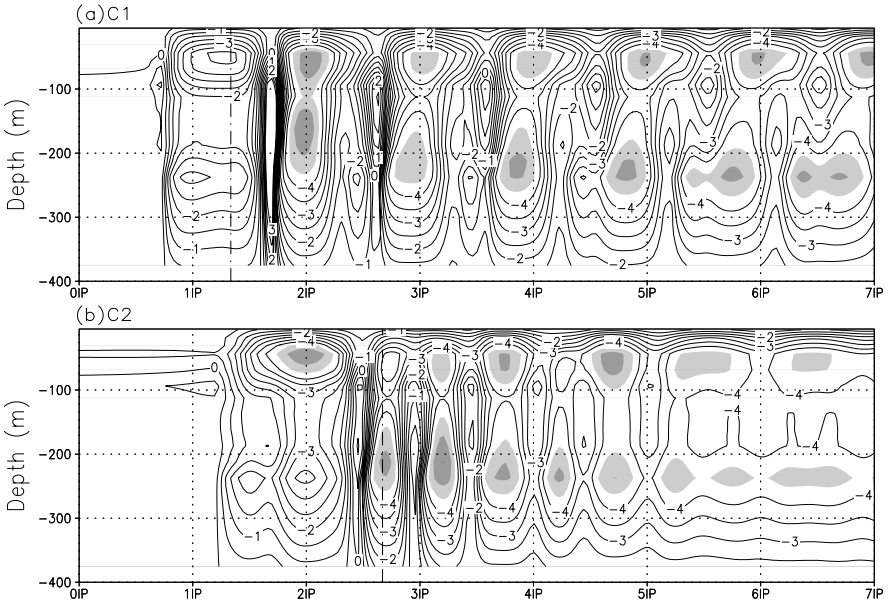

Fig. 6. Comparison of the cooling profiles of C1 (a) and C2 (b) for 0~7 IP at (119°E, 25.6°N). Contour interval is 0.5°C. Cooling exceeding 4.5°C is depicted by shaded areas. Dot-dashed lines mark the end of the wind-forced period and the beginning of the relaxation wake period.

the use of a no surface flux condition together with a strong upwelling may yield a solution with the cold water outcropping to the sea surface. This kind of thermal structure will never restore to the original state after the passage of the storm event. We therefore chose another option, the clamped SST condition, to force the near surface temperature field return to its initial state after the passing of a storm event. Certainly the clamped SST condition will generate an artificial temperature gradient near the sea surface, which is unfavorable to the surface cooling, so the meaning of the long time duration of the cooling event in case C1 then becomes more significant.

3.2 Momentum transfer

The intense, persistent inertial pumping in C1 is supported by the large wind-energy input in the forced period. In this resonant event the downward energy may penetrate the thermocline and initialize the motion there, which in turn drives the motion in the ML. The slab ML model used in previous, similar studies cannot describe this process because it either ignores the thermocline motion or simulates the entrainment as a one-way process (e.g. Chang and Anthes, 1978). Therefore, the thermocline is also important in the study of storm-induced cooling, especially for the resonant case in which significant energy is transferred from the ML, with consequent slow decays.

Momentum budget analysis is performed to identify the process responsible for the downward energy transfer. Figure 9 plots the upper-ocean 0~6 IP temporal variations in the vertical diffusion, vertical advection, horizontal advection, and Coriolis force terms in the momentum equation. The pressure gradient term in both cases is much smaller than these four terms in the upper ocean. In comparison, C1 appears to have stronger, deeper, and longer momentum variations than C2, particularly in the wake period, during which the inertial motion develops. Among those major momentum terms in the forced period, vertical diffusion contributes the most in both cases, although it reduces significantly after 2 IP. Note that the vertical diffusion process responds almost immediately to the wind, and the penetration depth is twice as deep in C1 as in C2 (Fig. 9(a)). It is noteworthy that such a difference in the penetration depth occurs within the ML and cannot be resolved when the ML is simulated as one single layer. With the downward diffusion of momentum we observe a corresponding increase in the Coriolis force term in the first 0.5 IP. The vertical advection term also contributes significantly to the momentum transfer in both cases. There is a delay of about half of the forced period for this term to respond to the wind. Although the advection terms are large in the forced period, their maxima occur at the first wave in the wake period with a vertical penetration depth that is much deeper in C1. The analysis thus revealed that when the pressure gradient term has negligible influence, diffusion and advection serve as the coupling mechanisms between the ML and the thermocline. Plueddemann and Farrar (2006) evalu-

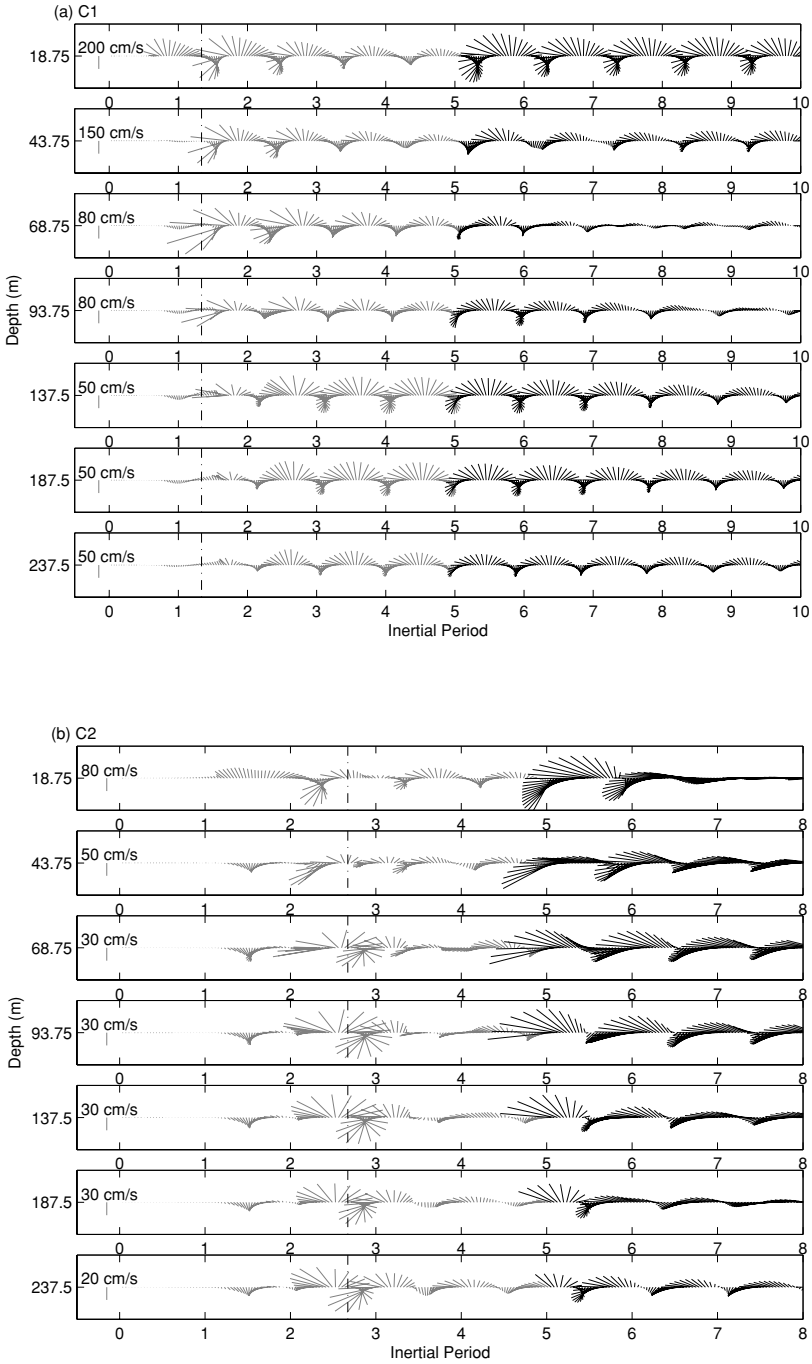

Fig. 7. Mean current velocity time series at seven layers for C1 (a) and C2 (b) at 119°E, 25~26°N. To better illustrate the current structure, the vector scale is not fixed in 0~5/4.5 IP in C1/C2 (current vector shown in gray color). For the remaining time, the scale is fixed at 50/10 cm/s in C1/C2 (current vector shown in black color). Dot-dashed lines mark the end of the wind-forced period and the beginning of the relaxation wake period.

ated the slab model performance and found that for strong resonant events, the kinetic energy balance in the slab ML model is unrealistic due to the lack of a damping mechanism to transfer momentum between the ML and a transition layer below. They found that the time scale needed for this mechanism to be effective is only a fraction of an IP, which is consistent with the diffusion process time scale in our results.

4. Discussion

4.1 Vertical mixing contributed cooling

The results in C1 and C2 suggest that when wind-current resonance occurs, a significant amount of momentum is transferred downward. For such events, vertical mixing is of great importance to the subsequent motions and cooling in the upper ocean. This can be demonstrated by additional numerical experiments with limited vertical mixing ability. Cases 1a and 2(a) contrast to C1 and C2, respectively, in that a constant vertical eddy viscosity is applied to the calculations. Figure 10(a) shows the vertical profile of the temperature differences for these two pairs; the profile illustrates the relative importance of mixing under different storm translation speeds. In the forced period, C1-C1a exhibits large differences at a depth near two cooling centers with a maximum temperature difference of 2°C in the ML base. In the wake period, the temperature difference increases to as much as 3°C and appears at a depth of around 180 m, where the vertical current shear is at a maximum. For slow-moving cases C2-C2a in the forced period, mixing is also intense in the ML base, in which the temperature difference reaches a maximum value of 2°C. The maximum difference then decreases to about 1.2~1.5°C in the wake period and shifts to a lower layer at 100~200 m. The mid-thermocline continues to be the most affected layer. Overall, the temperature differences between C2 and C2a are less significant, which indicates that the main cooling mechanism for C2 is upwelling. The cooling in C1, on the other hand, is more mixing-dominant, where the application of a constant vertical eddy viscosity results in much weaker cooling. In fact, the difference between the 6~7 IP averaged temperature profiles (Fig. 8(b)) of C1 and C2 serves to illustrate this point, too. This figure shows that distinct cooling is observed in the layer from 50~200 m, where the cooling depends greatly on the ocean's mixing ability. Since the upwelling in C2 is stronger, the entire water column is cooled more uniformly, except in the surface layer, where the influence of a fixed SST boundary condition is large. Nonetheless, in C1, the mixing effectively decreases the temperature in the ML base and a compensating warming effect reduces the cooling magnitude in this layer.

Along the cross-track direction, the temperature difference for (C1, C1a) and (C2, C2a) points to the same conclusion, namely, restricted vertical mixing has less effect on the cooling in slow-moving cases (Fig. 10(b)). The upper 50-m averaged temperature difference appears mainly on the right-hand side of the storm track, indicating that the mixing is mostly associated with the inertial motion. Along 25.6°N (main cooling center), the temperature change caused by different vertical mixing efficiencies is distinct only in the forced period. None-

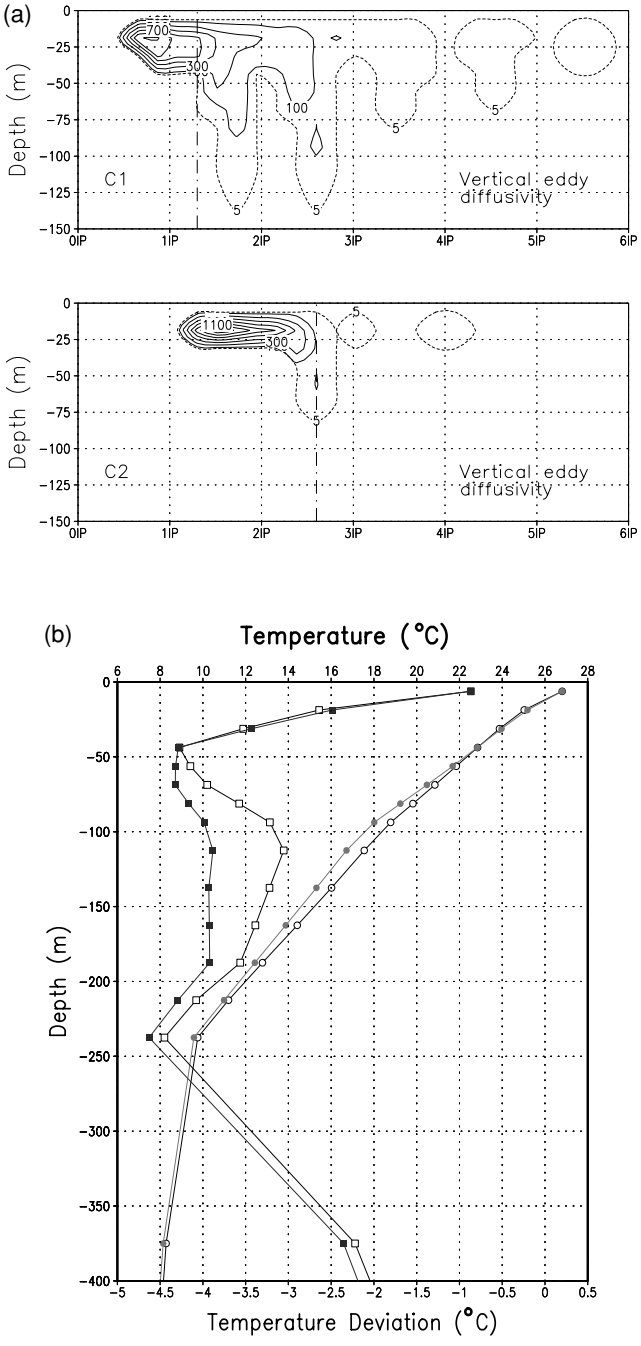

Fig. 8. (a) Time series of the magnitude of the vertical eddy diffusivity in the upper 150 m for C1 (upper panel) and C2 (lower panel) at (119°E, 25.6°N). Units are cm^2/s. Solid contour interval is 200. Dotted line is contour value 5, which is the value used in constant vertical eddy diffusivity run. Dot-dashed lines mark the end of the wind-forced period and the beginning of the relaxation wake period. (b) Comparison of 6~7 IP averaged temperature anomaly (line with squares) and temperature profiles (line with circles) for C1 (open symbol) and C2 (closed symbol) at (119°E, 25.6°N).

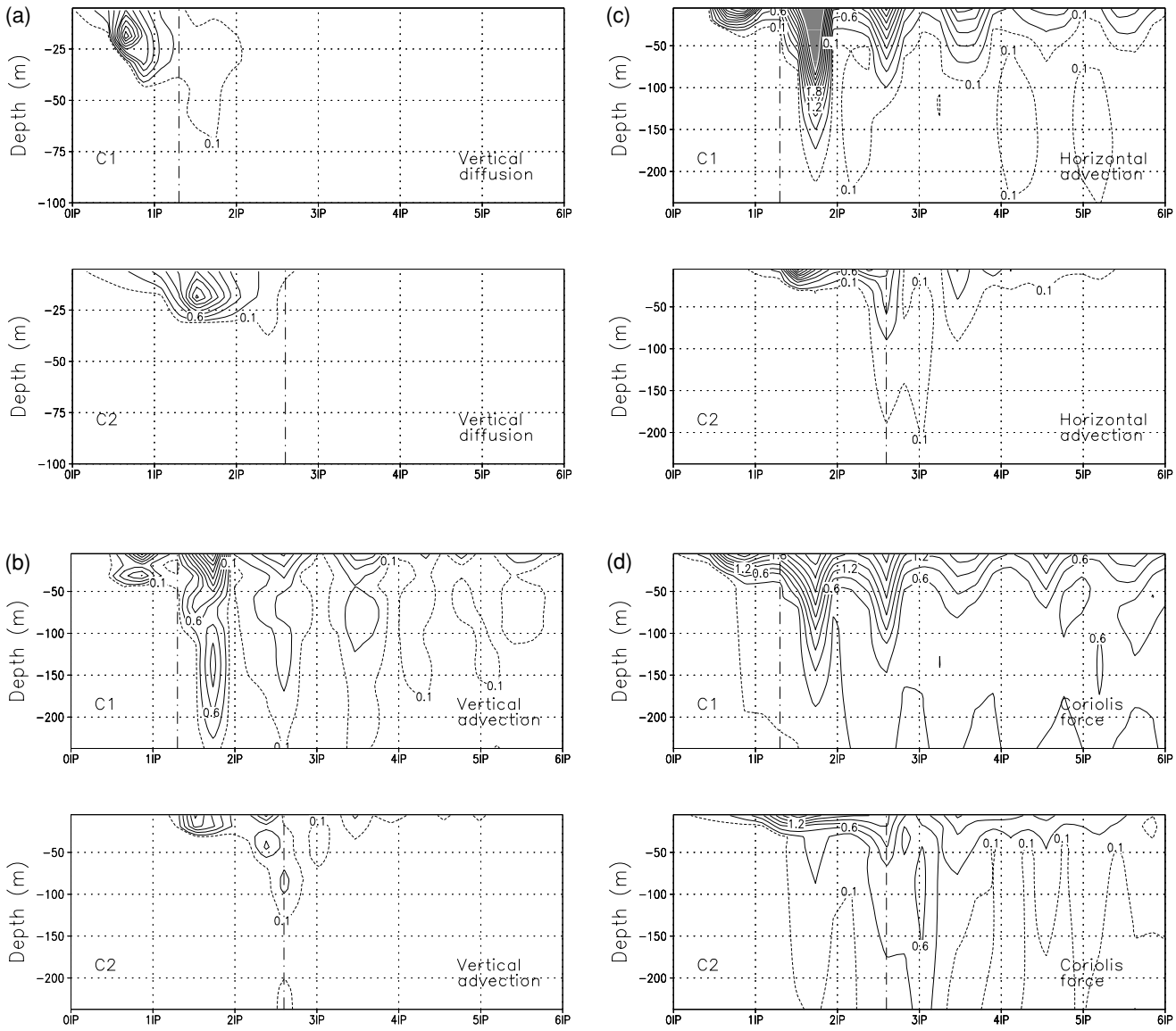

Fig. 9. (a) Time series of the magnitude of the momentum vertical diffusion in the upper 100 m for C1 (upper panel) and C2 (lower panel) at (119°E, 25.6°N). Units are 10^{-2} cm/s^2. Starting value and interval of the solid contour are both 0.3. Dotted line is contour value 0.1. Dot-dashed lines mark the end of the wind-forced period and the beginning of the relaxation wake period. (b) As (a) except for vertical advection. Note that the depth is extended to 250 m. (c) As (b) except for horizontal advection. Note that areas in gray correspond to values above 2.7. (d) As (b) except for Coriolis force.

theless, an interesting feature is observed in C1-C1a, namely, the temperature difference centered at 26~27°N fluctuates in the wake period with a maximum as high as 1.5°C. When compared with Fig. 5, it is evident that this feature corresponds to the second cooling center of C1. With limited vertical mixing, less energy is input to the lower layers, which results in the smaller inertial motion and reduced wake scale. Therefore, the second cooling center in C1a is significantly weaker than that in C1 and becomes the most distinct near-surface temperature discrepancy between them.

4.2 Storm residence time and wind-current coupling

Price *et al.* (1994) suggested that the storm-induced ocean cooling can be evaluated through the discussion of three nondimensional parameters: the storm speed S, the Burger number B, and the Rossby number Q. Both B and Q contain the ML thickness as a parameter in their calcu-

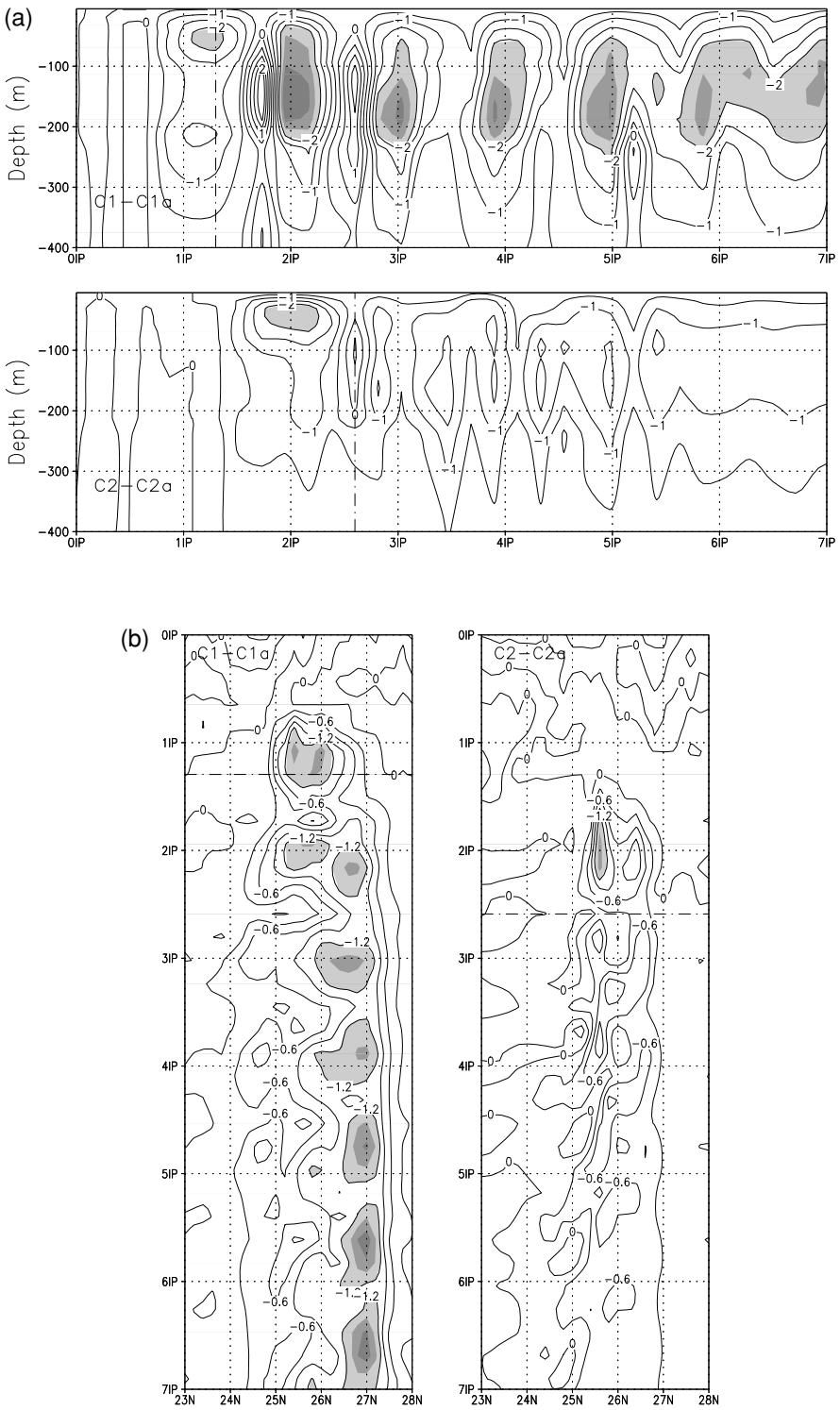

Fig. 10. (a) Comparison of the differences in the cooling profiles for C1-C1a (upper panel) and C2-C2a (lower panel) in 0~7 IP at (119°E, 25.6°N). Contour interval is 0.5°C. Cooling exceeding 2°C is depicted by shaded area. Dot-dashed lines mark the end of the wind-forced period and the beginning of the relaxation wake period. (b) Comparison of the upper 50-m mean temperature difference of the cross-track transect at 119°E for C1-C1a (left) and C2-C2a (right) from 0 to 7 IP. Contour interval is 0.3°C. Cooling exceeding 1.2°C is depicted by shaded areas. Dot-dashed lines mark the end of the wind-forced period and the beginning of the relaxation wake period.

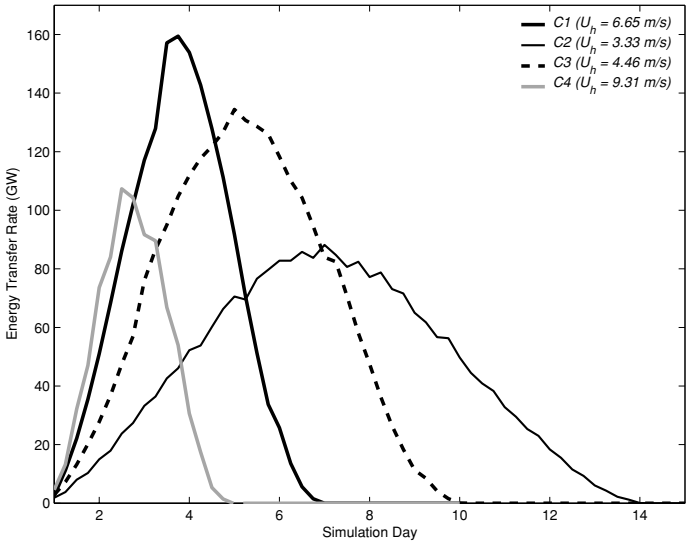

Fig. 11. Wind-to-ocean energy transfer rate for cases C1, C2, C3, and C4.

lations to indicate the entrainment and upwelling strength. On the other hand, S can be determined solely by external storm parameters. Wada (2005) presented a dataset of SST cooling and all three parameters are evaluated. It is shown that a rapid SST cooling was accompanied by an increase of Burger number and another period of cooling correlates well with an increase of Rossby number. According to our model results, the increasing B indicates an entrainment active response, so that S should suggest a wind-current resonant condition, while an increasing Q indicates an upwelling-dominated response when the condition reverses. The S value calculated from the storm dataset indeed is closer to 1 when B is increasing and is much smaller when Q is increasing. In other words, the cooling mechanism induced by a storm's passage can be inferred from the value of S, but other parameters are needed to better quantify the cooling strength.

The importance of S arises because different storm speeds result in a forcing of different frequencies and the ocean responds accordingly. The major factor in generating a strong and persistent wake is the wind-current resonance. It is known that the resonant response of the ocean occurs as the wind fluctuation approaches the inertial frequency; therefore, a nondimensional parameter such as S is proposed to evaluate this condition. Greatbatch (1984) introduced a parameter $k = U_h/Lf$, which measures the ratio of the local IP ($1/f$) to the storm residence time T_s (L/U_h). The nondimensional storm speed $S = \pi U_h/4fR_{\max}$ introduced by Price *et al*. (1994) also measures this ratio. The difference here is that Price chose the radius of the maximum wind, $R_{\max}$, as the storm scale while in Greatbatch's study, L was estimated to be $2.4R_{\max}$ based on the specific storm structure and wind stress field adopted. In this study, k is calculated in storm-affected regions as the ratio of the local inertial period to the period when the wind is greater than 1 dyne/cm^2 (i.e., IP/T_s). The results at the point (119°E, 25°N) for C1, C2, and two additional cases of U_h = 4.46 and 9.31 m/s are shown in Table 1. The k value increases with the storm speed or with a shorter residence time and it is closest to 1 in C4 among the four cases. The value of k suggests that the C4 case satisfies the resonant condition most closely, and should have the most intense response. However, comparison of the wind-to-ocean energy transfer rate for the entire storm with respect to time for these four cases shows that C4 is a weak, quick-passage case (Fig. 11). It is in C1 that a high transfer rate is observed, which is evident from the resonant response of the ocean to the moving storm.

The parameter k thus may not be a good indicator of the resonant response for the fastest storm case, because k measures the wind-current coupling based on the calculation of the rotation time scale only, whereas some important factors, such as the phase lag or velocity magnitude, are not considered. In fact, the level of wind-current coupling in our experiments can be evaluated by the wind-to-ocean energy input rate, which is equal to the inner product of the wind stress and the surface current. To further illustrate the drawbacks of considering the coupling based only on partial data, we can compare both the magnitude of the inner product and the cosine value of the angle between the wind stress and current vectors for the four cases. The cosine value measures how these two vectors coincide with each other in direction, while the amount of energy actually entering the ocean is determined by the energy transfer rate. Figure 12(a) shows

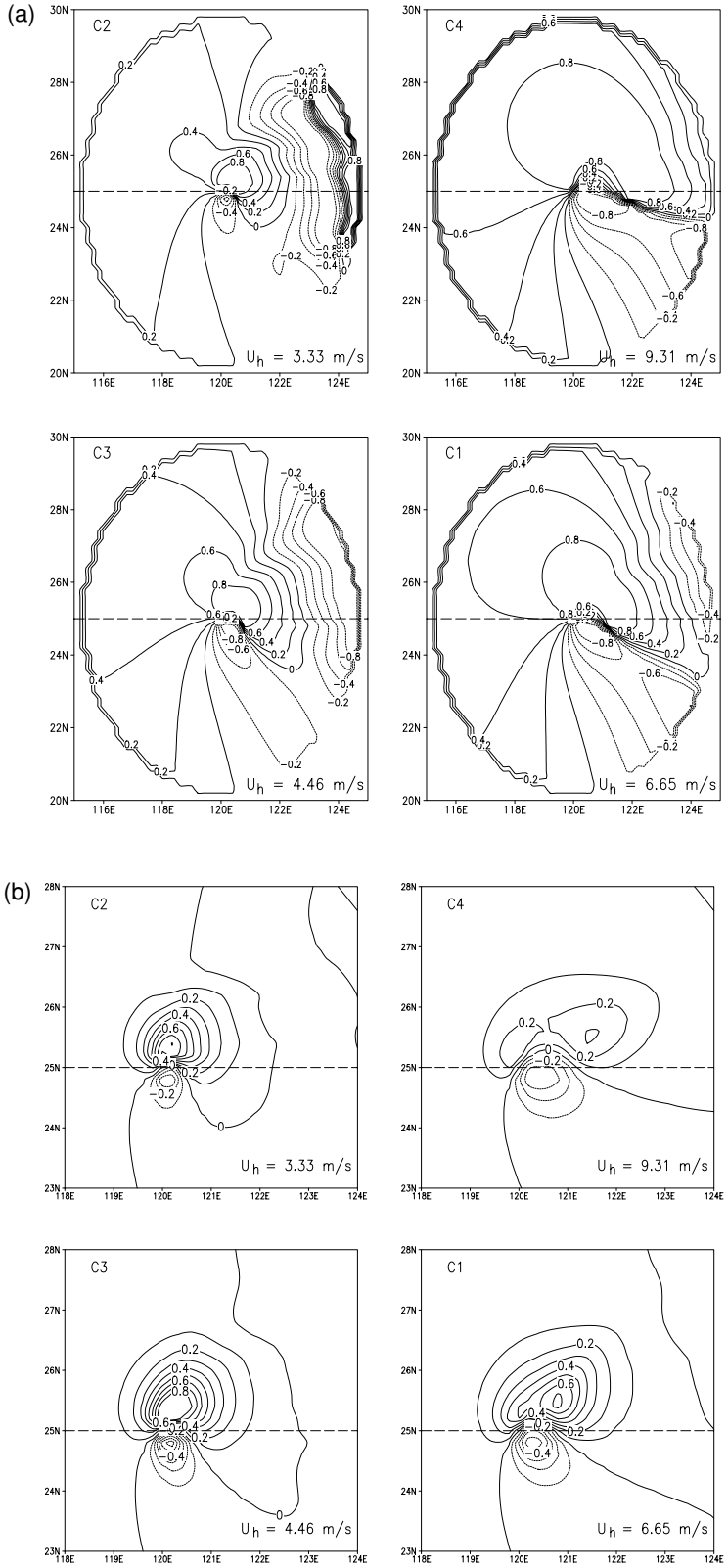

Fig. 12. (a) Distribution of the cosine of the angle between wind stress and surface currents for storms with different translation speeds. The storm center is located around (120°E, 25°N). Negative values are denoted by dotted lines. (b) Distribution of the wind energy transfer rate in mW/cm^2 for storms with different translation speeds. The storm center is located around (120°E, 25°N). The contour interval is 0.1 and the negative value is depicted by the dotted line.

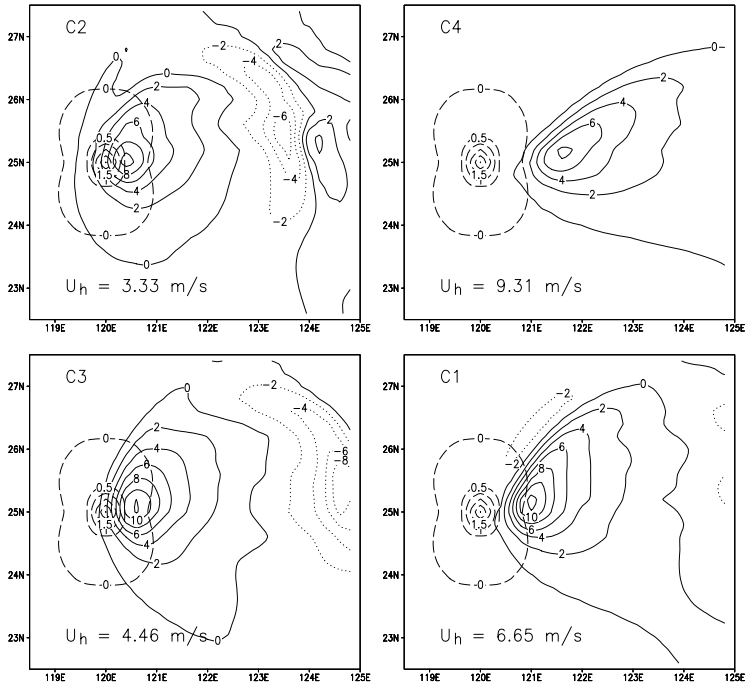

Fig. 13. Wind stress curl (dashed line, unit $10 \times$ dyne/cm^3) and current divergence (solid and dotted line, unit 10 s^{-1}) for storms with different translation speeds. Storm center is located around (120°E, 25°N).

the distribution of the cosine values when the storm is at the domain center, and Fig. 12(b) shows the corresponding energy transfer rate per unit area. The cosine value plot is quite similar to figure 16 in Price (1981), in that the stress is well coupled to the inertial currents on the right-hand side of a moving storm. The coupling is particularly good in the rear right quarter of a storm because in this region a current divergence center emerges at a distance from the storm center and the currents are thus turning in the same direction as the wind stress. It is evident that the vector direction coupling in the storm improves with increasing U_h such that, for the fastest storm case, only the left rear quarter has a negative value. The coverage and magnitude of the positive value area becomes smaller when U_h decreases and the negative value area grows out from the right rear quarter. This negative value area corresponds to the region where the current veers opposite to the wind stress, which is the following convergence center. An alternate positive and negative area of cosine values for a storm with a smaller value of U_h is merely the result of a smaller along-track response scale, wherein the current already turns a cycle, from divergence to convergence, within the wind affected area.

Nonetheless, good directional coupling, such as that in the fastest moving case C4, does not necessarily produce higher energy transfer rates. In case C4, the current divergence center is so remote from the storm center that the strong wind stress region does not overlap with the strong current region (Fig. 13) and the directional coupling in the strong wind region near the storm center even becomes negative (Fig. 12). The transfer rate of wind energy into the ocean in this case is thus the smallest among all cases. Therefore, under identical wind stress distributions, the wind-current coupling depends on the location of the first current divergence center generated behind the storm. The faster the storm moves, the farther away the divergence center emerges behind the storm. The resonant response may not be inferred directly by the parameter k because in a sense it represents only the directional coupling. An overlap of the large current region with the maximum wind region is also required for large energy transfer into the ocean.

A good indicator of the degree of overlap is the relative distance between the storm center and the first current divergence center. This distance is estimated to be approximately 15%~20% of the along-track response scale with increasing storm translation speeds. Figure 14 shows the correlation of the storm speed and the mean distance between the storm center and the first current divergence center for four cases. Their relationship appears to be linear and the factor between them, which is a scale of time, is about 1/4 IP. This result is consistent with the fact that, after the onset of a wind field, the surface wind-driven current will sense the earth's rotation effect only after a quarter of the local inertial period. As the inertial current emerges in the ocean response, the

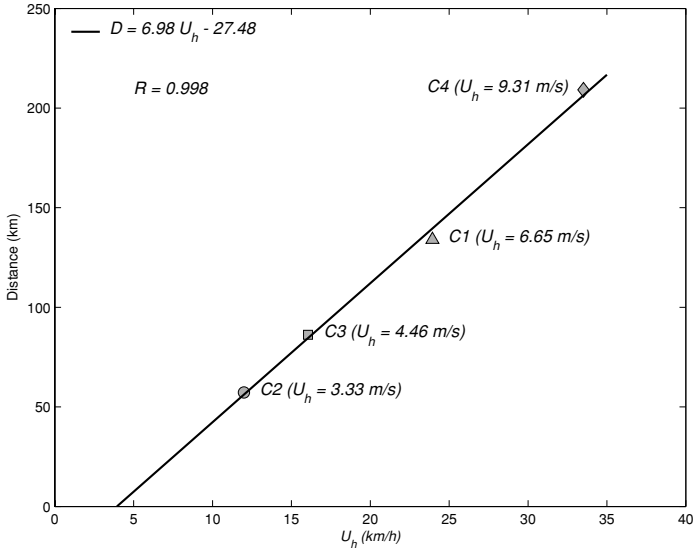

Fig. 14. Distance between storm center and first current divergence center for storms with different translation speeds. Distance is averaged over 21 sampling points uniformly distributed between about 105~135°E for each case except case 4, which includes only 15 data points due to its rapid translation speed. Solid line is linear regression line and R is correlation coefficient for the data set.

storm center already travels a distance of the order ($U_h \times$ 1/4 IP) downstream. The inertial current in the upper ocean will continue to receive energy input from the wind field only when the storm is sufficiently great and there is still appreciable overlap between the active wind region and the underlying inertial current field, together with the proper directional coupling (C1 in Fig. 13).

5. Conclusion

The upper ocean cooling induced by the passage of a typhoon is studied using a 3-D primitive equation model with higher vertical resolution in the ML and the thermocline. The model retains the diffusion process, which was often simplified in previous similar studies, and uses the level-2 turbulence closure scheme to determine the vertical eddy viscosity and simulate the vertical mixing. The results of numerical experiments with various storm translation speeds show that the cooling intensity by vertical mixing depends on whether or not resonant wind-current coupling is induced. Considerable downward momentum transfer occurs for resonance events through the diffusion and advection processes when the pressure gradient is negligible. The inertial motions in the thermocline developed from this energy input, and the vertical structure of horizontal velocity are dominated by the first baroclinic mode in a few IPs. As the currents in the ML and the thermocline established such coupling, the inertial pumping in the upper ocean could then persist for a longer duration into the wake period. This kind of feedback from the thermocline to the ML cannot be obtained from the slab ML model since it models the entrainment as a one-way process. For cases of weak wind-current coupling, the downward energy transfer is restricted and weak and thus the inertial oscillations decay rapidly. This type of response is generally observed in mid- and high-latitude regions because the residence time for a typical typhoon (i.e., size 500 km moving at 5.5 m/s) is usually longer than the local inertial period. On the other hand, a C1-type response is more frequently seen in low-latitude region is because the inertial period is longer and the resonance condition is easier to achieve. This is why the ocean current data observed from many moored instruments deployed in the South China Sea show large downward energy transfer in several typhoon passage events (Chen, 2006).

In either case, the storm-induced cooling is mainly set up in the forced period. The temperature decrease in this period is larger for the slow-moving storm because of greater upwelling from a longer residence time. This process allows the entire water column in the upper ocean to cool uniformly. The mixing contributed cooling is similar in the ML of both cases but larger in the thermocline of the fast-moving case. In addition, in the fast-moving case when the wind-current resonance occurs, the active mixing supported by the strong, persistent inertial current vertical shear can enhance the ML cooling in the relaxation period. The temperature decrease in the upper thermocline then reduces slightly as a result of the mixing process. With no significant vertical shear generated in the slow-moving case, the ML gradually warms up in

the wake period and the inertial current decays in 4~5 IP—a typical time scale for the observed storm response events. Model simulations show that the slow-moving and the resonant fast-moving cases can lead to similar cooling intensities in the ML and the lower thermocline over a longer time period. In the layer between them, the mean temperature is higher for the resonant case because of the stronger entrainment mixing.

The conventional nondimensional storm speed is evaluated using the model results. This parameter is used to measure the degree of wind-current coupling and is calculated as the ratio between the storm wind rotation time scale and the local inertial period. Since its concept is based on the time scale only, a displacement of the maximum current region from the maximum wind stress region by increasing the storm translation speed eventually leads this parameter to fail. In such extreme cases, the wind stress and current vectors may have good directional coupling, as indicated by this parameter, but the wind work is in fact far from a resonance condition.

Acknowledgements

This work was sponsored by the National Science Council, the Republic of China, Grant NSC 95-2611-M002-015-MY3.

References

Chang, S. W. and R. A. Anthes (1978): Numerical simulations of the ocean's nonlinear baroclinic response to translating hurricanes. *J. Phys. Oceanogr.*, **8**, 468–480.

Chen, Y. K. (2006): Typhoon induced inertial motion in the South China Sea. Master thesis, Institute of Oceanography, National Taiwan University, 98 pp. (in Chinese).

Cione, J. J. and E. W. Uhlhorn (2003): Sea surface temperature variability in hurricanes: implications with respect to intensity change. *Mon. Wea. Rev.*, **131**, 1783–1796.

Crawford, G. B. and W. G. Large (1996): A numerical investigation of resonant inertial response of the ocean to wind forcing. *J. Phys. Oceanogr.*, **26**, 873–891.

D'Asaro, E. A. (2003): The ocean boundary layer below Hurricane Dennis. *J. Phys. Oceanogr.*, **33**, 561–579.

Emanuel, K. (2001): Contribution of tropical cyclones to meridional heat transport by the oceans. *J. Geophys. Res.*, **106**, D14, 14771–14781.

Geisler, J. E. (1970): Linear theory of the response of a two-layer ocean to a moving hurricane. *Geophys. Fluid Dyn.*, **1**, 249–272.

Greatbatch, R. J. (1984): On the response of the ocean to a moving storm: parameters and scales. *J. Phys. Oceanogr.*, **14**, 59–78.

Holland, G. J. (1980): An analytic model of the wind and pressure profiles in hurricanes. *Mon. Wea. Rev.*, **108**, 1212–1218.

Jocob, S. D., L. K. Shay and A. J. Mariano (2000): The 3D oceanic mixed layer response to Hurricane Gilbert. *J. Phys. Oceanogr.*, **30**, 1407–1429.

Mellor, G. L. and P. A. Durbin (1975): The structure and dynamics of the ocean surface mixed layer. *J. Phys. Oceanogr.*, **5**, 718–728.

Plueddemann, A. J. and J. T. Farrar (2006): Observations and models of the energy flux from the wind to mixed-layer inertial currents. *Deep-Sea Res. II*, **53**, 5–30.

Pollard, R. T. and R. C. Millard, Jr. (1970): Comparison between observed and simulated wind-generated inertial oscillations. *Deep-Sea Res.*, **17**, 813–821.

Price, J. F. (1981): Upper ocean response to a hurricane. *J. Phys. Oceanogr.*, **11**, 153–175.

Price, J. F. (1983): Internal wave wake of a moving storm. Part I: scales energy budget and observations. *J. Phys. Oceanogr.*, **13**, 949–965.

Price, J. F., T. B. Sanford and G. Z. Forristall (1994): Forced stage response to a moving hurricane. *J. Phys. Oceanogr.*, **24**, 233–260.

Semtner, A. J. and Y. Mintz (1977): Numerical simulation of the Gulf Stream and mid-ocean eddies. *J. Phys. Oceanogr.*, **7**, 208–230.

Shay, L. K., R. L. Elsberry and P. G. Black (1989): Vertical structure of the ocean current response to a hurricane. *J. Phys. Oceanogr.*, **19**, 649–669.

Wada, A. (2002): The processes of SST cooling by typhoon passage and case study of typhoon Rex with a mixed layer ocean model. *Pap. Meteor. Geophys.*, **52**, 31–66.

Wada, A. (2005): Numerical simulations of sea surface cooling by a mixed layer model during the passage of typhoon Rex. *J. Oceanogr.*, **61**, 41–57.

Zedler, S. E., T. D. Dickey, S. C. Doney, J. F. Price, X. Yu and G. L. Mellor (2002): Analyses and simulations of the upper ocean's response to Hurricane Felix at the Bermuda Testbed Mooring site: 13–23 August 1995. *J. Geophys. Res.*, **107**, C12, 3232, doi:10.1029/2001JC000969.